**Fig. 12** The same patient of Fig. 11. **A and B** : T1 weighted axial (**A**) and coronal (**B**) slices with enhancement before treatment A high and low-signaled mass (**arrow heads**) was visible at the suprasellar cistern. The low-signaled edema-like change (**arrow**) was noted along the left optic tract. **C** : Heavily T2 weighted axial slice at the one slice above the optic tract before treatment. The edema-like changes (**arrows**) were visible bilaterally along the optic tract. The left side was more prominent. **D** : Heavily T2 weighted coronal slice before treatment. The edema-like changes (**large arrows**) were visible bilaterally along the optic tract. The optic tracts were difficult to differentiate from the edema-like changes. On the right side, a curvilinear vessel-like high signal (**red arrow**), originating from the edema-like change, was visible. **E** : Heavily T2 weighted axial slice above the level of the optic tract, 3 months after surgery (similar slice level to **C**). The edema-like change disappeared completely on the right side. Large perivascular spaces (**large arrow**), present in normal conditions, were visible on the same side. The edema-like change (**small arrow**) seemed to remain on the left side. **F** : Heavily T2 weighted coronal slice, 3 month after surgery (similar slice level to **D**). A large perivascular space was visible on the right optic tract (**large arrow**). A slight degree of the edema-like change (**small arrow**) remained on the left side.

脳腫瘍にも生じうると報告した [35,36] (**Fig. 12, 13, 14**). さらに治療前後の冠状断の微細な観察から, 視索付近に生理的に存在する血管周囲腔に沿った分布をしていることを報告した. 胚細胞腫, 悪性リンパ腫, 転移性脳腫瘍, 頭蓋咽頭腫などに高頻度にみられることから, 下垂体腫瘍の中でも侵潤度が高く癒着を起こしやすい腫瘍に特徴的に出現しやすい傾向がある [35,36].

Saeki らは視索沿いの浮腫様変化の発生機転を以下のように推論している. まず, 正常解剖脳の視索を含む冠状断の組織学的検索を行った. 結果

として全例に視索沿いに大きな血管周囲腔が存在し [7], 付近のくも膜下腔と交通していることを証明した [36] (**Fig. 15, 16**). 血管周囲腔は, 脳内の細胞外液がくも膜下腔に流れ込む際, 通路の役割を果たすことが知られている. 血管周囲腔の内容液の流れる方向から, 静脈系の流出路の障害とすると理解しやすい. これらを総合的に鑑みて, 視索付近に生理的に存在する血管周囲腔と脳底部のくも膜下腔との交通路が腫瘍により遮断された結果, 本来血管周囲腔を介してくも膜下腔に流れ込む細胞外液 (組織液) が関連した局所の血管周囲
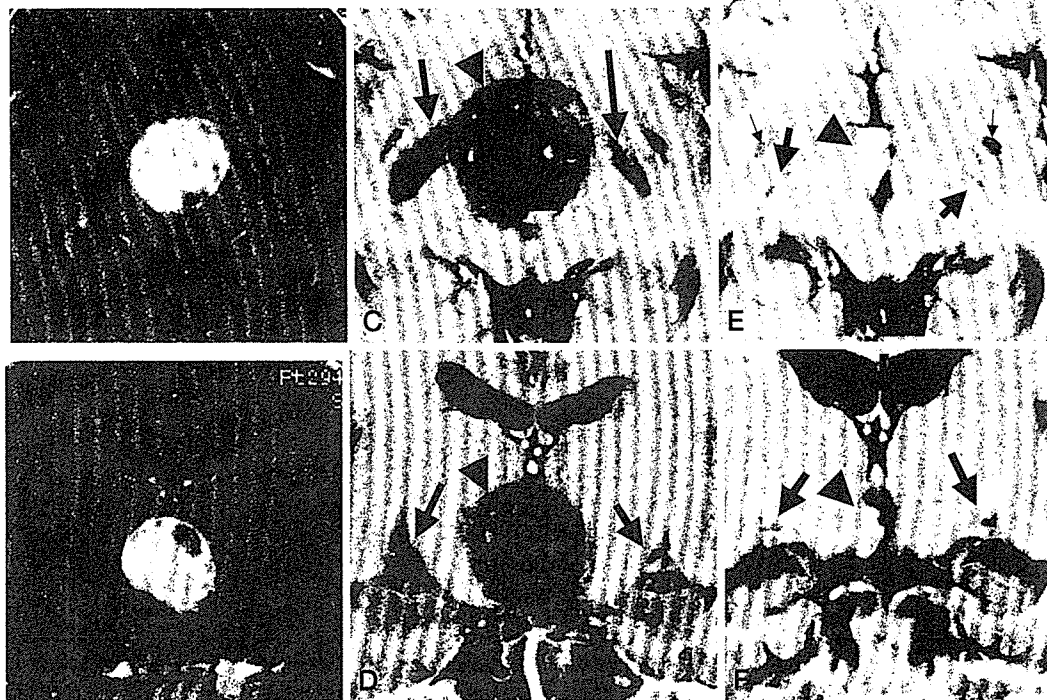
Fig. 13 A 11-year-old boy with a germ cell tumor. **A and B** : T1 weighted axial (**A**) and coronal (**B**) slices with contrast enhancement. A round and almost high-signaled mass (**arrow heads**) was visible at the suprasellar region. The edema-like change along the optic tract was visible bilaterally in the axial section and on the right side in the coronal section (**arrows**). **C and D** : Heavily T2 weighted axial and coronal MR images before treatment. Moderate and slight edema-like changes (**arrows**) were visible along the right and left optic tracts, respectively. The tumor (**arrow head**) was visible. **E** : Heavily T2 weighted axial slice above the level of the optic tract 2 months after treatment (similar slice level to **C**). The edema-like change disappeared completely bilaterally, although the tumor (**arrow head**) remained in the third ventricle. Normally present large perivascular spaces (**large arrows**) were visible. Large perivascular spaces associated with anterior perforated substance were visible (**small arrows**). **F** : Heavily T2 weighted coronal slice 2 month after treatment (similar slice level to **D**). Large perivascular spaces (**arrows**) were bilaterally visible on the optic tracts. The tumor remained in the third ventricle (**arrow head**).

腔に沿って停滞・貯留した状態であるとしている[36)] (**Fig. 17**). これは, 鞍上部くも膜下腔での脳脊髄液の局所的循環障害が脳実質内に浮腫様変化を来したとするものである. 脳脊髄液の循環障害が中枢神経に浮腫様変化を来すことは, キアリ奇形に伴う脊髄空洞症で報告されている[10)] (**Fig. 18**). キアリ奇形例において大後頭孔の減圧術で脊髄空洞症が改善し, 画像上の上部頸髄の浮腫様変化が消失したことが報告されている[10)]. 動物実験でも同様に, 上部頸髄のくも膜下腔の脳脊髄液の循環障害で付近の浮腫様変化を認め, 組織学的に血管周囲腔の拡大を認めた[10)]. 以上のごとく, 局所の脳脊髄液循環障害で浮腫様変化を来す可能

性が, 視索付近と上部頸髄で報告された.

従来, 脳浮腫の機序として cytotoxic edema と vasogenic edema, その他が報告されている[22)]. われわれが渉猟し得た範囲では, 局所の脳脊髄液循環障害が浮腫様変化を来すとする報告はみられない. 新しい脳浮腫の発生機転である可能性があり, 今後, さらに動物実験, 人生体での画像所見による病態の解明, より高磁場の画像による検討などが必要である.

VI. 最後に

MR の解像度の向上に伴い, 血管周囲腔にまつわる種々の病態が明らかとなってきた. 今後, 3
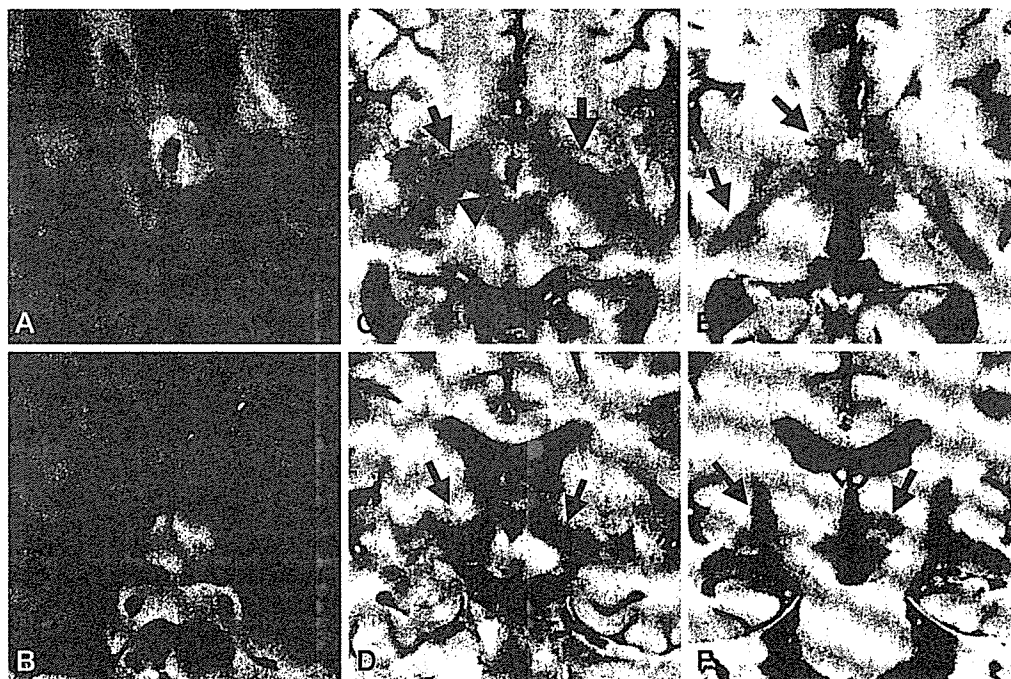
Fig. 14 A 62-year-old man with malignant lymphoma. **A and B** : T1 weighted axial (**A**) and coronal (**B**) slices with enhancement, before treatment. A high-and low-signaled mass (**arrow heads**) was visible in the third ventricle. The low-signaled edema-like changes (**large arrows**) were noted along the optic tracts. A venous angioma was incidentally found in the left anterior basal ganglia (**small arrow**). **C-F** : Heavily T2 weighted axial (**C, E**) and coronal (**D, F**) slices before treatment. In **C**, the tumor (**arrow head**) was visible. Marked edema-like changes were visible in the hypothalamus and midbrain and along the optic tracts (**arrows**). The edema-like change extends to the perivascular spaces related to the anterior perforated substances (**red arrows**). In **D**, the tumor (**arrow head**) was visible. Marked edema-like changes were visible in the hypothalamus and along the optic tract (**arrows**). In **E** and **F**, the edema-like changes (**arrows**) extended as far as to the basal ganglia and the internal capsule. In **F**, marked edema-like change was visible in the hypothalamus and midbrain (**arrows**).
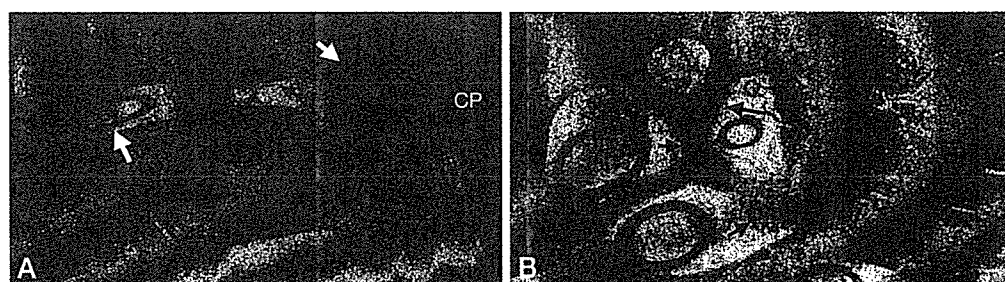
Fig. 15 Histologic materials from a 79-year-old female without CNS lesions. **A** : Coronal section of the middle portion of the optic tract at the slice showing the cerebral peduncle (**CP**). Haematoxylin and eosin stain. X 20. Along the optic tract (**OT**), there is a large space, 1.5 mm in height, which possesses the following features. A pial layer (**black arrow**) lines the inner surface. Vessels (**white arrows**) are present in the space, and no necrotic or ischemic changes are visible at the surrounding brain tissue. The histologic features are compatible with those of perivascular spaces around the anterior commissure in Fig. 15B. Small spaces(**arrow heads**) are also present adjacent to the optic tract. **B** : Coronal section at the anterior commissure (**AC**) and the lower basal ganglia with multiple perivascular spaces. Haematoxylin and eosin stain. X 40. Adjacent to the anterior commissure, there are multiple perivascular spaces, which include vessels and are lined by pial layer (**arrows**). No necrotic or ischemic changes are visible in the surrounding brain tissue.
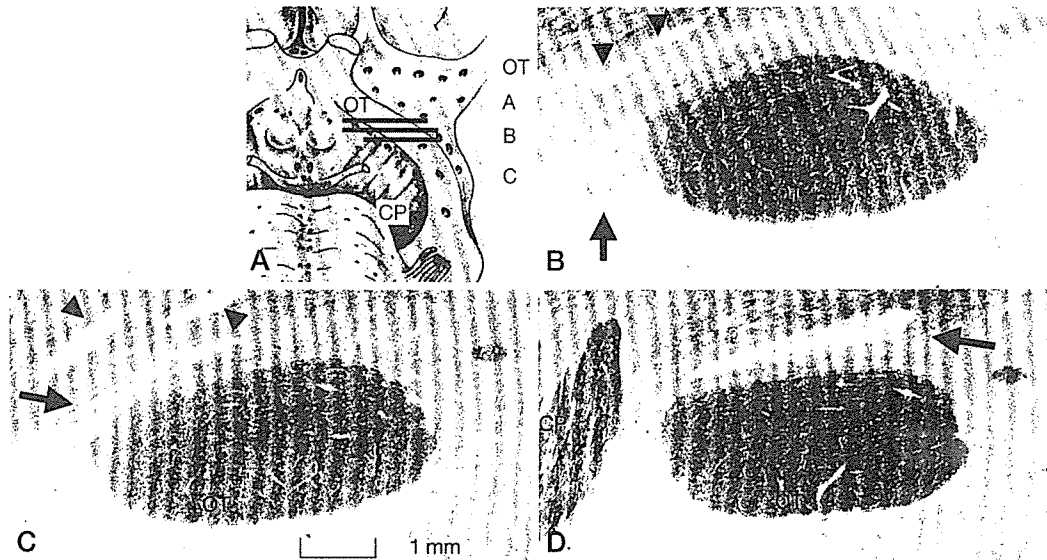
Fig. 16 Histologic materials from a 86-year-old female without CNS lesion. **A** : A picture showing 3 lines, which correspond to the slice locations of Fig.16B, C and D. **B to D** : Kluver and Barrera technique x 25. Continuous thin sections of penetrating vessel (arrows) from the perforation point at the subarachnoid space (**B**) to the largest peri-vascular space adjacent to the optic tract (**C and D**). Its maximum height is 0.5 mm. These show the perforation point medial to the optic tract and perivascular space along the optic tract communicates the adjacent subarachnoid space. [Abbreviation] **OT**: optic tract, **CP**: cerebral peduncle.
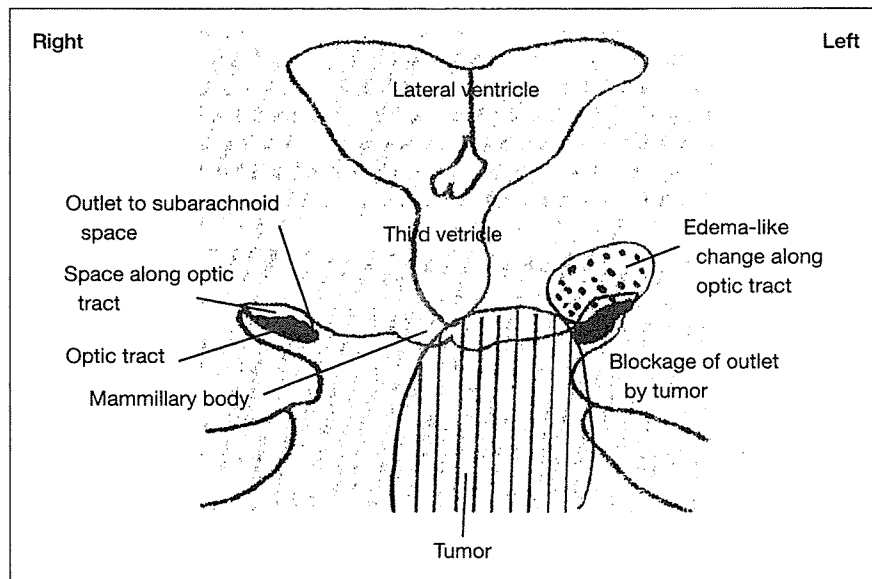
Fig. 17 Original scheme showing a possibly new mechanism for the edema-like change along the optic tract in pituitary region tumors. The normal anatomy is shown on the right side and a pituitary region tumor on the left side. On the right side, the perivascular space along the optic tract is shown to communicate with the adjacent subarachnoid space through a thin channel, located at the medial to the optic tract. On the left side, a tumor in the pituitary region blocks the outlet (channel) from the perivascular space along the optic tract to the subarachnoid space, mechanically, due to inflammation or adhesive processes. Thus, interstitial fluid retention occurs in the perivascular spaces, which distends along the optic tract (dotted area).

Fig. 18 Presyrinx state in a patient with Chiari malformation (from reference 10). Sagittal T1 weighted image (500/14/3) Cord expansion and parenchymal hypointensity are present in the upper cervical cord. Sagittal T2 weighted image (3000/105/3) Marked upper cervical cord T2 prolongation. This was presumed to trelated to ongoing or increased obstruction to CSF flow. This MR images show that subarachnoid CSF flow disturbance may cause intraparenchymal edema-like change in the upper spinal cord.
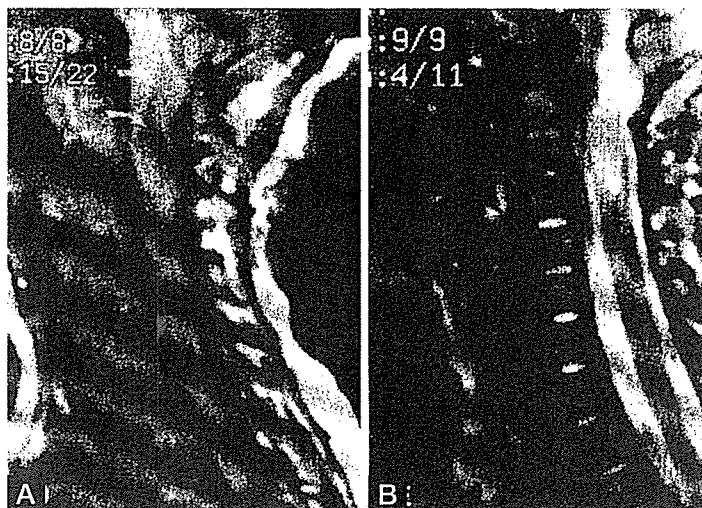
テスラーMR機などより高磁場の機器がさらに普及していくことから，血管周囲腔を含めた種々の病態が解明されていくことを期待したい．

文　献

1) Achiron A, Faibel M : Sandlike appearance of Virchow-Robin spaces in early multiple sclerosis : a novel neuroradiologic marker. AJNR Am J Neuroradiol 23 : 376-380, 2002

2) Adachi M, Hosoya T, Haku T, Yamaguchi K : Dilated Virchow-Robin spaces : MRI pathological study. Neuroradiology 40 : 27-31, 1998

3) Benhaiem-Sigaux N, Gray F, Gherardi R, et al : Expanding cerebellar lacunaes due to dilatation of the perivascular space asociated with Binswanger's subcortical arteriosclerotic encephalopathy. Stroke 18 : 1087-1092, 1987

4) Bradbury MW, Cserr HF, Westrop RJ : Drainage of cerebral interstitial fluid into deep cervical lymph of the rabbit. Am J Physiol 240 : F329-F336, 1981

5) Braffman BH, Zimmerman RA, Trojanowski JQ, Gonatas NK, Hickey WF, Schlaepfer WW : Brain MR : Pathologic correlation with gross and histopathology. 1 lacuanar infarction and Virchow-Robin spaces. AJNR Am J Neuroradiol 8 : 621-628, 1988

6) Davis GA, Fitt GJ, Kalnins RM, Mitchell LA : Increased perivascular spaces mimicking frontal lobe tumor. J Neurosurg 97 : 723, 2002

7) DeArmond S, Fusco MM, Dewey MM : Structure of human brain. Oxford Press, New York, 1976, p26

8) Elster Ad, Richardson DN : Focal high signal on MR scans of the midbrain caused by enlarged perivascular spaces : MR-pathologic correlation. AJNR Am J Neuroradiol 11 : 1119-1122, 1991

9) Esiri MM, Gay D : Immunological and neuropathological significance of the Virchow-Robin space. J Neurol Sci 100 : 3-8, 1990

10) Fischbein, NJ, Dillon WP, Cobbs C, Weinstein PH : The "presyrinx" state : a reversible myelopathic condition that may precede syringomyelia. AJNR Am J Neuroradioloy : 20 : 7-20, 1999

11) Heier LA, Bauer CJ, Schwartz L : Large Virchow-Robin spaces : MR-clinical correlation. AJNR Am J Neuroradiol 10 : 929-936, 1989

12) Higashi S, Yamashita J, Fujisawa H, Yamamoto Y, Kadoya M : Moustache appearance in craniopharyngiomas : unique magnetic resonance imaging and computed tomographic findings of perifocal edema. Neurosurgery 27 : 993-996, 1990

13) Homeyer P, Cornu P, Lucette L, Chiras J, Derouesne C : A special form of cerebral lacunae : expanding lacunae. J Neurol Neurosurg Psychiatry 611 : 200-202, 1996

14) Kanamalla US, Calabro F, Jinkins JR : Cavernous dilatation of mesencephalic Virchow-Robin spaces with obstructive hydrocephalus. Neuroradiol 42 : 881-884, 2000

15) Jungreis CA, Kanal E, Hirsch WL, Martinez AJ, Moossy J : Normal perivascular spaces mimicking lacunar infarction : MR imaging. Radiology 169 : 101-104, 1988

16) Kalimo H, Kaste M, Haltia M : Vascular diseases In Graham DI, Lantos PL eds., Greenfield's Neuropathology vol 1 Sixth edition. Arnold, London, 1997,

pp315-396

17) Komiyama M, Yasui T, Izumi T : magnetic resonance imaging features of unusually dilated Virchow-Robin spaces? two case reports-. Neurol Med Chir(Tokyo) **338** : 161-164, 1998

18) Mai JK, Assheuer J, Paxinos G : Atlas of the human brain. San Diego, Academic Press, 1997, pp160-216

19) Mamata Y, Muro I, Matsumae M, Komiya T, Toyama H, Tsugane R, Sato O : Magnetic resonance cisternography for visualization of intracisternal fine structures. J Neurosurg **88** : 670-678, 1998

20) Maclullich AM, Wardlaw JM, Ferguson KJ, Starr JM, Seckl JR, Deary IJ : Enlarged perivascular spaces are associated with cognitive function in healthy elderly men. Neurol Neurosurg Psychiatry **75** : 1519-1523, 2004

21) Mascalchi M, Salvi F, Godano U, Nistri M, Taiuti R, Tosetti M, Villari N, Calbucci F : Expanding lacunae causing triventricular hydrocephalus. Report of two cases. J Neurosurg **91** : 669-674, 1999

22) Miller JD, Ironside JW : Raised intracranial pressure oedema and hydrocephalus. In Graham DI, Lantos PL eds., Greenfield's Neuropathology vol 1 Sixth edition. Arnold, London, 1997, pp157-195

23) 水谷俊雄 : 脳の血管周囲腔―血管周囲腔の病理形態学. 脳神経 **52** : 661-669, 2000

24) Nagahata M, Hosoya T, Kayama T, Yamaguchi K : Edema along the optic tract : useful MR finding for the diagnosis of craniopharyngiomas. AJNR Am J Neuroradiol **19** : 1753-1757, 1998

25) Ogawa T, Okudera T, Fukasawa H, Hashimoto M, Inugami A, Fujita H, Hatazawa J, Shimosegawa E, Noguchi K, Uemura K : Unusual widening of Virchow-Robin spaces : MR appearance. AJNR Am J Neuroradiol **16** : 1238-1242, 1995

26) Ohta H, Kojima N, Ihara N, Ishigaki T, Todo G, Okamoto S : MR and Tc HMPAO SPECT images in a case of unusual widening of perivascular spaces (Virchow-Robin spaces). Annals of Nuclear Medicine **13** : 437-439, 1999

27) Ono Y, Suzuki M, Kayama T, Yoshimoto T : Multilobulated cystic formation in the brain stem with Benedikt's syndrome : case report. Neurosurgery **34** : 726-729, 1994

28) 奥寺利夫, 田村 元, 上村和夫 : 脳の血管周囲腔―映像上から―. 脳神経 **52** : 671-690, 2000

29) Parent A : Carpenter's human Neuroanatomy 9th edition. Williams and Wilkins, Baltimore, 1996, p13

30) Poirier J, Barbizet J, Gaston A, Meyrignac C : Thalamic dementia. Expansive lacunae of the paramedian thalamo-mesencephalic territory. Hydrocephalus caused by stenosis of the aqueduct of Sylvian. Rev Neurol (Paris) **139** : 349-358, 1983

31) Rennels M, Gregory TF, Blaumanis O, Fujimoto K,

Grady PA : Evidence of a paravascular fluid circulation in the mammalian central nervous system, provided by the rapid distribution of tracer protein throughout the brain to the subarachnoid space. Brain Res **326** : 47-63, 1985

32) Romi F, Tysnes OB, Krakenes J, Savoiardo M, Aarli JA, Bindoff L : Cystic dilatation of Virchow-Robin spaces in the midbrain. Eur Neurol **47** : 186-188, 2002

33) Saeki N, Rhoton AL Jr : Microsurgical anatomy of the upper basilar artery and the posterior circle of Willis. J Neurosurg **46** : 563-578, 1977

34) Saeki N, Kubota M, Murai H, Yamaura A : Unusually widened perivascular spaces in the cerebral hemisphere : the importance of MRI for diagnosis of a benign clinical entity. Br J Neurosurg **17** : 576-577, 2003

35) Saeki N, Uchino Y, Murai H, Kubota M, Isobe K, Uno T, Sunami K, Yamaura A : MR study on edema-like change along the optic tract in patients with pituitary region tumors. AJNR Am J Neuroradiol **24** : 336-342, 2003

36) Saeki N Nagai Y, Matsuura I, Uchino Y, Kubota M, Murai H, Ishikura H, Ikehira H, Yamaura A : Histologic characteristics of normal peivascular spaces along the optic tract : New pathogenetic mechanism for edema in tumors in the pituitary region. AJNR Am J Neuroradiol **25** : 1218-1222, 2004

37) Saeki N, Sato M, Kubota M, Uchino Y, MUrai H, Nagai Y, Ishikura H, Nomura S, Matsuura S, Yamaura A : MR imaging of normal perivascular space at midbrain. AJNR Am J Neuroradiol **26** : 566-571, 2005

38) Salamom G : Atlas of the arteries of the human brain. Paris France, Sandoz Edition, 1971, p121

39) Schick S, Gahleitner A, Wober-Bingol C, Wober C, Ba-Ssalamah A, Schoder M, Schindler E, Prayer D : Virchow-Robin spaces in childhood migarine. Neuroradiology **41** : 283-287, 1999

40) Schroeder HWS, Gaab MR, Warzok RW. Endoscopic treatment of an unusual multicystic lesion of the brain stem : case report. Br J Neurosurg **10** : 193-196, 1996

41) Weller RO, Kida S, Zhang E : Pathways of fluid drainage from the brain-morphological aspects and immunological significance in rat and man. Brain Pathol **2** : 277-284, 1992

42) Wilkins RH, Burger PC : Benign intraparenchymal brain cysts without an epithelial lining. J Neurosurg **68** : 378-382, 1998

43) Youl BD, Plant GT, Stevens JM, Kendall BE, Symon L, Crockard HA : Three cases of craniopharyngioma showing optic tract hypersignal on MRI. Neurology **40** : 1416-1419, 1990

44) Zhang ET, Inman CBE, Weller RO : Interrelationships of the pia mater and the perivascular spaces in the human cerebrum. J Anat **170** : 111-123, 1990

Dissociated expressive and receptive language functions on magnetoencephalography, functional magnetic resonance imaging, and amobarbital studies

Case report and review of the literature

Kyousuke Kamada, M.D., Fumiya Takeuchi, M.D., Shinya Kuriki, M.D., Tomoki Todo, M.D., Akio Morita, M.D., and Yutaka Sawamura, M.D.

Department of Neurosurgery, Faculty of Medicine, The University of Tokyo; and Department of Neurosurgery and Research Institute for Electronic Science, Hokkaido University, Sapporo, Japan

✓ Dissociated language functions are largely invalidated by standard techniques such as the amobarbital test and cortical stimulation. Language studies in which magnetoencephalography (MEG) and functional magnetic resonance (fMR) imaging are used to record data while the patient performs lexicosemantic tasks have enabled researchers to perform independent brain mapping for temporal and frontal language functions (MEG is used for temporal and fMR imaging for frontal functions). In this case report, the authors describe a right-handed patient in whom a right-sided insular glioma was diagnosed. The patient had a right-lateralized receptive language area, but expressive language function was identified in the left hemisphere on fMR imaging– and MEG-based mapping. Examinations were performed in 20 right-handed patients with low-grade gliomas (control group) for careful comparison with and interpretation of this patient's results. In these tests, all patients were asked to generate verbs related to acoustically presented nouns (verb generation) for fMR imaging, and to categorize as abstract or concrete a set of visually presented words consisting of three Japanese letters for fMR imaging and MEG.

The most prominent display of fMR imaging activation by the verb-generation task was observed in the left inferior and middle frontal gyri in all participants, including the patient presented here. Estimated dipoles identified with the abstract/concrete categorization task were concentrated in the superior temporal and supramarginal gyri in the left hemisphere in all control patients. In this patient, however, the right superior temporal region demonstrated significantly stronger activations on MEG and fMR imaging with the abstract/concrete categorization task. Suspected dissociation of the language functions was successfully mapped with these two imaging modalities and was validated by the modified amobarbital test and the postoperative neurological status. The authors describe detailed functional profiles obtained in this patient and review the cases of four previously described patients in whom dissociated language functions were found.

Key Words • amobarbital test • functional magnetic resonance imaging • magnetoencephalography • language mapping • language function

B RAIN asymmetries have been of considerable interest in the field of neurology for more than a century. A classic mode of language organization based on lesional studies proposes a frontal expressive area, named for Broca, for planning and executing speech and writing, and a posterior receptive area, named for Wernicke, for analysis and identification of linguistic sensory stimuli. This basic scheme of language function has been generally accepted, with the assumption that both of the classic language functions exist only in the dominant hemisphere.

The amobarbital test is currently used to determine language dominance, but requires catheterization of the carotid arteries and successive anesthetization of each hemisphere by unilateral injections of sodium amobarbital. Data from previous studies have indicated that among right-handed participants, 4% have speech dominance generally in the right hemisphere, and in 90% it is found in the left hemisphere.[3] Several studies in which this technique was used have shown an increased incidence of atypical language dominance patterns in patients with injury in the left hemisphere. These patterns have been interpreted in terms of

---

Abbreviations used in this paper: BVRT = Benton Visual Retention Test; fMR = functional magnetic resonance; ICA = internal carotid artery; IQ = intelligence quotient; MEG = magnetoencephalography; WAB = Western Aphasia Battery; WAIS-R = Wechsler Adult Intelligence Scale–Revised.

interhemispheral language transfer and cerebral plasticity.[6,20] The amobarbital test, however, measures only the relative distribution of language across the two hemispheres and is not usually repeatable. More specific information and careful interpretation between hemispheres are practically and scientifically important factors for understanding the language networks.

The recently developed fMR imaging modality has been used to identify the dominant hemisphere for language functions. Most fMR imaging studies of language location have shown frontal activation in the inferior and middle frontal gyri during performance of various tasks, such as verb (word) generation and word categorization.[15,22,27] Although several authors have attempted to detect the receptive language function with fMR imaging by using listening or sentence comprehension tasks, only a few pixels revealing activation have been observed in the temporoparietal region.[8,15,23,24] Therefore, empirical evidence has shown that temporal activation is more difficult to detect than frontal activation. In addition, a fundamental limitation of fMR imaging–based brain mapping involves the varying degrees of regional hemodynamic responses in pathological brain conditions.[7,9,14] Therefore, the interpretation of fMR imaging–based localization for receptive language function remains difficult and controversial.

The MEG modality reflects the intracellular flow of electrical current in the brain and allows accurate localization of the current's dipole sources. Regarding language function, Papanicolaou and colleagues[17,18] localized MEG deflections, which peaked at approximately 400 msec after word presentation (late responses), in the temporoparietal regions. These investigators suggested that the late responses were strongly related to receptive language function. We have also reported dense dipole clusters of the semantic late responses in the superior temporal, supramarginal, and fusiform gyri of the suspected dominant hemisphere.[11,12] Therefore, MEG is a powerful diagnostic tool for identifying language dominance and the Wernicke area.

Given these findings, we have used fMR imaging and MEG modalities to visualize the expressive and receptive language functions independently and to identify the dominant hemisphere. In this case report, we describe a right-handed patient who had a right-sided insular glioma and a confirmed right-lateralized receptive language area, but in whom dissociated expressive function was found in the left hemisphere. The suspected dissociation of language functions was clearly mapped with fMR imaging and MEG, and was validated by the amobarbital test and the patient's postoperative neurological status. We describe detailed neurological and radiological findings characterizing the unusual functional organization in this patient, comparing these with the fMR imaging–MEG templates obtained in 20 control patients who underwent imaging in our institution. We also discuss the data acquired in four previously reported patients with dissociated language functions on fMR imaging–based brain mapping.

Case Report

History. This 29-year-old, right-handed man experienced amnesia for several minutes in November 2003. He has suffered from depression for 10 years and has been unemployed, despite the absence of neurological deficits. Computerized tomography scanning of the brain performed 11 years earlier had revealed no abnormality. The patient has been treated with several of the most commonly used tranquilizers in the outpatient clinic of our Department of Psychiatry. Neuropsychological examinations, including the WAIS-R and the BVRT, which were performed in April 1992, demonstrated no language deficit or memory disturbance, and the patient had a full-scale IQ of 86 (Table 1).

Neuroimaging, Neuropsychological Evaluation, and Surgical Planning. In November 2003, T_1-weighted MR images revealed a hypointense mass in the right insular cortex involving the surrounding white matter. The lesion was homogeneously hyperintense on T_2-weighted MR images and was not enhanced by addition of Gd–diethylenetriamine pentaacetic acid (Fig. 1A). These findings suggested that a

TABLE 1
Sequential results of neuropsychological examinations in a patient with dissociated language function*

| Test	Item	4/1/1992	11/2/2002 (preop)	3/3/2003 (postop)
WAIS-R	verbal IQ	95	98	90
	information	9	10	9
	digit span	8	9	8
	vocabulary	10	12	8
	arithmetic	6	6	6
	comprehension	12	12	8
	similarities	10	9	10
	performance IQ	76	75	74
	picture completion	8	7	8
	picture arrangement	11	8	8
	block design	6	8	5
	object assembly	7	9	8
	digit symbol	3	3	3
	full-scale IQ	86	87	82
BVRT	no. of errors (normal mean, 5)	2	5	7
WMT	memory quotient	93	101	105
WAB	aphasia quotient	NT	98.6	92.8

* NT = not tested; WMT = Wechsler memory test.
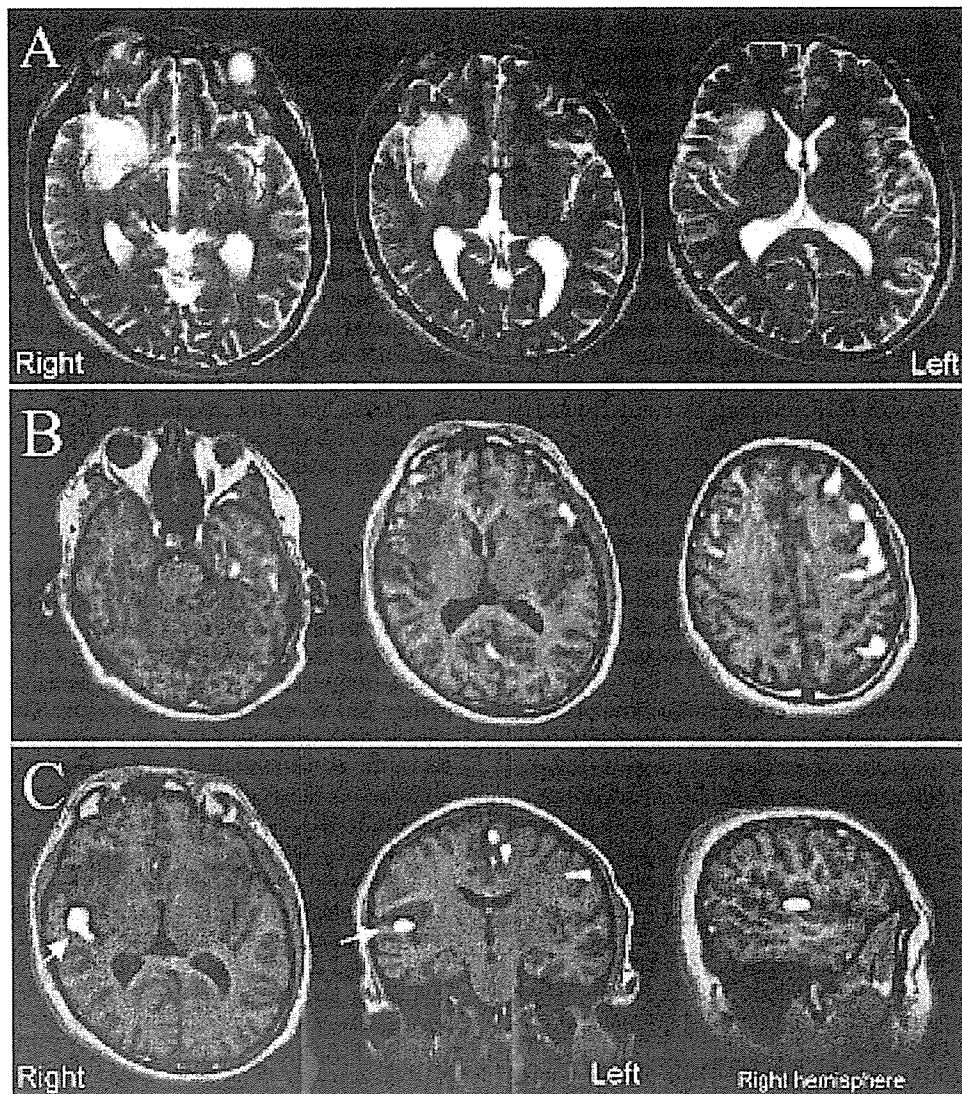
FIG. 1. A: Axial T_2-weighted MR images obtained in a 29-year-old man, demonstrating a right insular tumor. B: Brain activation measured using fMR imaging during the verb-generation task. The images display all activated areas with a Z-score of more than 2.2, which are mainly located in the inferior and middle frontal gyri. C: Activation on fMR images during the abstract/concrete categorization task, demonstrating right-sided dominance in the superior temporal region (arrows). The dissociated language function is observed in the left frontal and right temporal regions.

low-grade astrocytoma might have developed slowly over the past 11 years. The Edinburgh Handedness Inventory score was 114, indicating strong right-handed dominance. Preoperative neuropsychological examinations, including the WAB, in addition to the WAIS-R and BVRT, detected no language deficit or memory disturbance (Table 1). Performance IQ, verbal IQ, and memory function were unchanged from the previous examinations. Considering the tumor's location, the symptoms, and the patient's handedness, we planned to perform a radical resection.

Because we have previously reported elsewhere that postsurgical language deficits can be predicted based on results of MEG studies,[12] and have evaluated more than 70 patients by using both MEG and fMR imaging to identify the language dominance, this patient underwent functional brain mapping as usual. To obtain the standard language template for MEG and fMR imaging–based brain mapping, we selected 20 control patients with low-grade gliomas (four tumors in the left frontal or right temporal lobe, and six in the left temporal or right frontal lobe). Eight gliomas involved the right and six involved the left insular region on T_2-weighted images. All patients in the control group had left-hemisphere language dominance, which was confirmed with the amobarbital test.

Protocols for MR Imaging. Anatomical MR and fMR imaging were performed during the same session with a 1.5-tesla whole-body MR unit equipped with echoplanar capabilities and a standard whole-head transmitter–receiver coil (Vision; Siemens, Erlangen, Germany). During the experiments, foam cushions were used to immobilize the patient's head.

Language Tasks Used for fMR Imaging. All language tasks that required responses were performed covertly. The fMR

images were acquired with a T_2-weighted echoplanar imaging sequence (TE 62 msec; TR 114 msec; flip angle 90°; slice thickness 4 mm; slice gap 2 mm; field of view 260 mm; matrix 64 × 128; 14 slices). Each fMR imaging session consisted of three dummy scan volumes, three activation periods, and four baseline (rest) periods. During each period, five echoplanar imaging volumes were collected, yielding a total of 38 imaging volumes. The fMR imaging data for language-related semantic responses were acquired as follows. All participants were examined using two different lexicosemantic language paradigms: 1) verb generation after acoustic presentation of nouns; and 2) abstract/concrete categorization of words after their presentation for reading. All words for semantic tasks were selected from common Japanese words listed in the electronic dictionary of the National Institute for Japanese Language.

Verb-Generation Task. For the verb-generation task, common concrete nouns were presented aurally. The auditory stimuli (duration range 400–600 msec) were produced by a native Japanese speaker with a flat intonation and were digitized, with a sampling rate of 44,000 Hz. Backward playback of the sound files was used to eliminate the primary auditory activation for the rest period with exactly the same interstimulus intervals (1600–2400 msec) as the active condition. The auditory stimuli were delivered binaurally through two 5-m-long plastic tubes terminating at a set of headphones. The sound intensity was an approximately 95-decibel sound pressure level at the participant's ear. Individuals were instructed to generate silently a verb related to each noun presented during the active periods.

Abstract/Concrete Categorization Task. Visual stimuli were presented on a liquid crystal display monitor, and a mirror positioned above the head coil allowed the patients to see the stimuli. During the abstract/concrete categorization task, words consisting of three kana letters (Japanese phonetic symbols) were presented with a 300-msec exposure time and an interstimulus interval ranging from 1800 to 2200 msec. Participants were instructed to categorize the presented word covertly as abstract or concrete. During the control period, they passively viewed random dots, which were created by destructuring kana letters and were controlled to have the same brightness as the kana words to eliminate primary visual responses. Before undergoing imaging studies, all participants had practiced briefly, and two fMR imaging examinations were performed for each task to confirm the consistency of results.

After data acquisition, a motion detection program (MEDx; Medical Numerics, Sterling, VA) discarded fMR sessions containing motion artifacts of more than 25% of the pixel size. After applying a gaussian spatial filter (7 mm in half width), functional activation maps were calculated by estimating Z-scores between the rest and activation periods with Dr. View software (Asahi Kasei, Tokyo, Japan). Clusters consisting of more than 10 pixels with a Z-score of higher than 2.2 were accepted as indicating real activation. The result of each fMR session was coregistered to three-dimensional T_1-weighted MR images of each participant's head, maximizing the mutual information of the data sets with the Affine transformation.[4,16]

Protocol for Lexicosemantic MEG. The MEG signals were recorded with a 204-channel biomagnetometer (Vector View; Neuromag, Helsinki, Finland) in a magnetically

shielded room. We repeatedly acquired two data sets with each task to confirm stability and the MEG responses on two different days (10 and 7 days before the operation). One hundred fifty words were presented visually with a 300-msec exposure time, with interstimulus intervals ranging from 2800 to 3200 msec during MEG recordings. Each word consisted of three kana letters and was grammatically a noun. All patients were asked to categorize the presented word as abstract or concrete, pushing a button with the index finger for an abstract word or with the middle finger for a concrete one (kana-reading task). To identify the lexicosemantic responses specific to the kana-reading task, we presented 150 pairs of Arabic letters and asked patients to decide whether each pair had the same letters or different ones (figure-discrimination task). All patients participated in brief practice sessions before the measurement. Each epoch consisted of a 500-msec prestimulus baseline and a 1500-msec analysis period following stimulus delivery. The averaged magnetic signals were digitally filtered between 0.1 and 30 Hz. Significant MEG deflections were visually identified on the basis of the root mean squared fields of more than 10 sensors in the frontotemporal or temporooccipital regions. Locations and moments of equivalent current dipoles were calculated every 2 msec from 250 to 600 msec after the stimulus onsets by using the single equivalent dipole model. Only dipoles with a correlation value of more than 0.90 were accepted and were superimposed onto three-dimensional T_1-weighted MR images by identifying anatomical fiduciary landmarks. To confirm the calculated results, the same MEG time sections were analyzed with one of the current density maps; this is called the multiple current estimate.[26]

Protocol for the Amobarbital Test. All patients received injections of amobarbital (100 mg in a 10% solution) through the ICA. Language testing was performed during the initial period of maximal amobarbital action, which was indicated by contralateral brachial plegia. The following tasks were included: Task I, spontaneous counting (patients started counting just before amobarbital injection and were told to continue counting until the investigator presented the next task); Task II, letter reading (patients were then told to read aloud seven words consisting of three or four kana letters); Task III, naming (patients were asked to name aloud five objects that were pictorially presented); Task IV, auditory comprehension (patients were asked to perform three simple tasks such as blinking their eyes, opening their mouth, and raising their unparalyzed arm); and Task V, pointing to objects (a table with pictures of four objects was presented, and patients were told to select one picture by pointing— "where is the rabbit," "point to the cat," and so on). Performance in Tasks I and III was considered to reflect the patient's expressive linguistic capacities, whereas Tasks II, IV, and V were used to screen receptive language functions.

Data Obtained in Control Patients

Findings on fMR Images. The regions activated by the verb-generation task were restricted mostly to the left hemisphere. The activated regions involved the inferior frontal gyrus and the middle frontal gyrus, the lateral precentral gyrus, the supramarginal gyrus, and the supplementary motor area. Although several activations were found on the right side, in the right middle frontal and lateral precentral
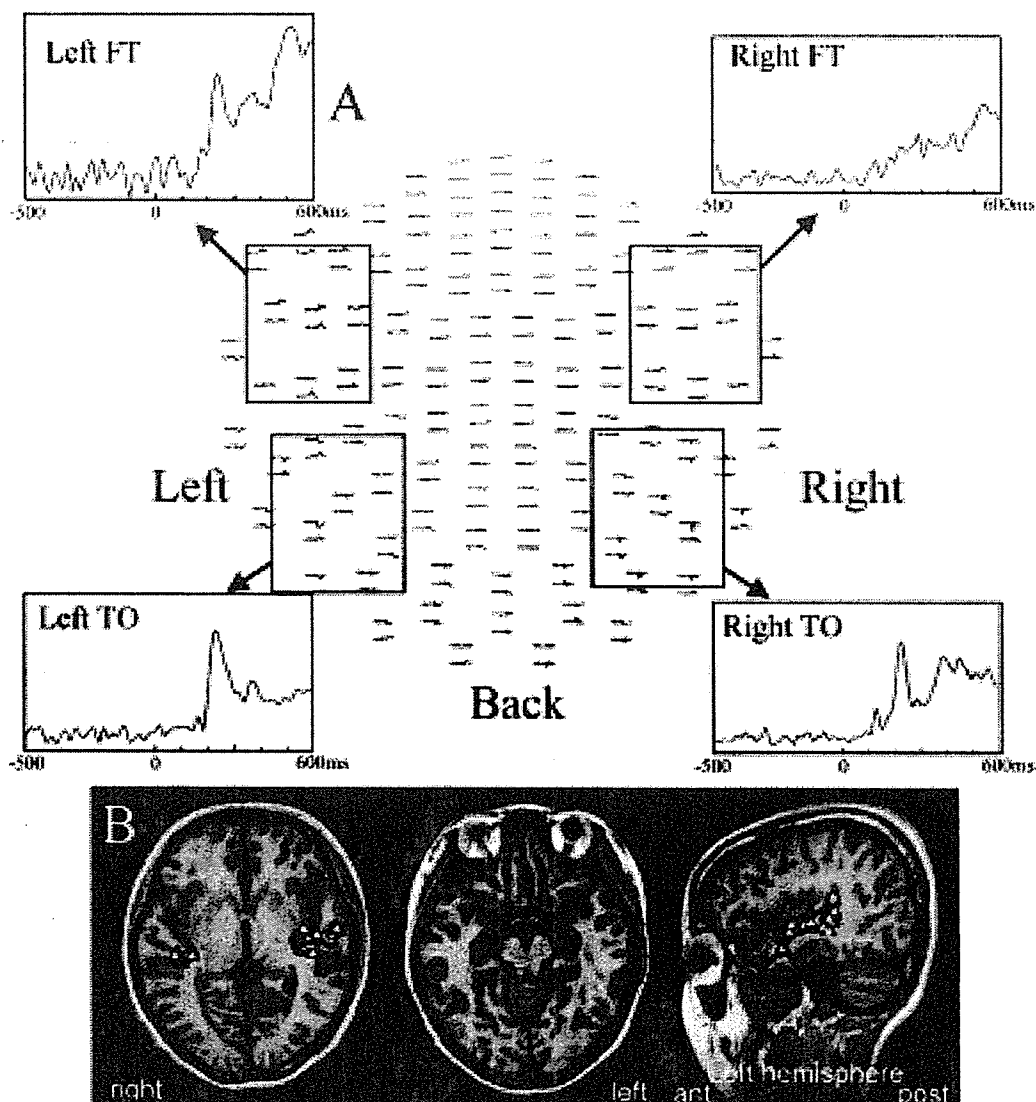
FIG. 2. A: Root mean squared profiles of lexicosemantic responses on both sides in the frontotemporal and temporooccipital regions on MEG studies obtained in a control patient. The left frontotemporal responses, peaking at 450 msec, are markedly larger in amplitude than the ones on the right. B: Neuroimages used in source localization of the late frontotemporal deflections, revealing predominant dipole clusters in the left superior temporal region. There are 107 dipoles in the left and 32 in the right hemisphere. FT = frontotemporal; ms = msec; TO = temporooccipital.

gyrus, they did not reach cluster significance (maximum values of Z-score < 2.2 or less than 10 pixels; data not shown). Although activations with the abstract/concrete categorization task tended to be lateralized to the left hemisphere, the bilateral frontal regions including the middle frontal and lateral precentral gyrus were involved. In addition, sporadically activated areas were found in the left superior temporal and the left fusiform gyri in seven of the 20 control patients.

The MEG Profiles and Dipole Locations. Figure 2 demonstrates results of imaging in a control patient. All patients were able to perform both tasks during data acquisitions. The values that follow are expressed as the means ± standard deviations. The mean reaction time and the rate of successful task performance in control patients were approximately 850.3 ± 32.4 msec and 94.2 ± 5.3%, respectively. In all control patients, the late deflections peaking at 400

msec were predominantly observed in the left rather than the right frontotemporal region (Fig. 2A). Bilateral temporooccipital regions demonstrated relatively early sharp deflections at approximately 250 msec with no hemispheral dominance in amplitude. As shown in Fig. 2B, the estimated dipoles of the frontotemporal regions were concentrated in the left superior temporal, middle temporal, and supramarginal gyri (the mean number of dipoles was 122.4 ± 24.2), whereas the right hemisphere showed far fewer dipoles (52.4 ± 14.2). In contrast, there were no significant hemispheral differences in the dipole concentration in the temporooccipital regions. Because the figure-discrimination task evoked only early deflections (within 300 msec) in both hemispheres with few late responses, on the basis of these results and previous reports, we speculate that late responses in the left hemisphere are strongly related to the lexicosemantic processes in letter perception.[11,12,18] In all control
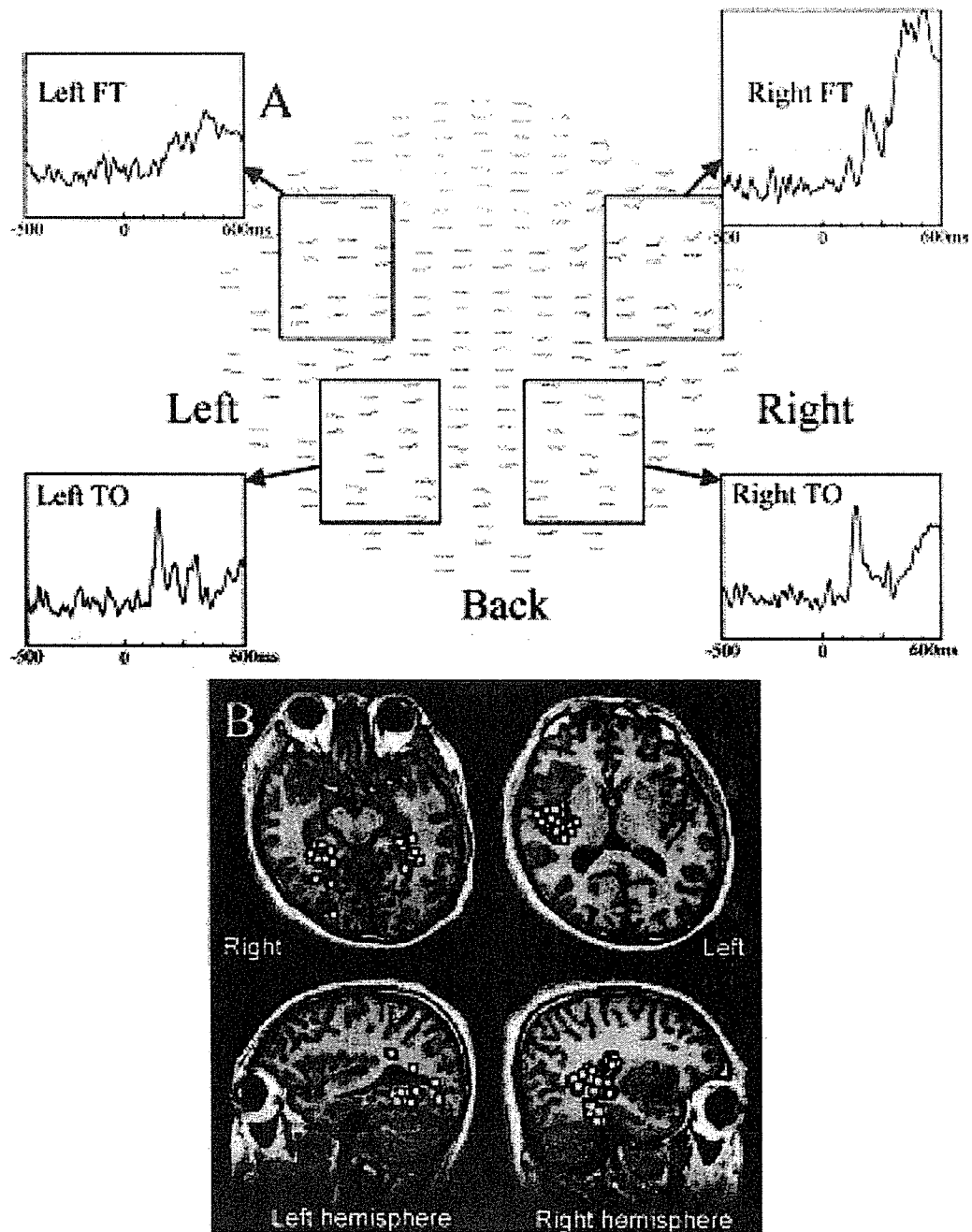
FIG. 3. A: Root mean squared profiles of lexicosemantic responses on both side in the frontotemporal and temporooccipital regions on MEG studies obtained in our patient. The right frontotemporal responses, peaking at 450 msec, are significantly larger in amplitude than the ones on the left. B: Neuroimages used in source localization of the late frontotemporal deflections, revealing predominant dipole clusters in the right superior and inferior temporal regions. There are 48 dipoles in the left and 202 in the right hemisphere.

patients, the activation profiles of fMR imaging and MEG studies clearly indicated left-sided dominance of the frontal expressive and temporal receptive language functions.

Data Obtained in Our Patient

Findings on fMR Images. The verb-generation task activated locations in our patient that were very similar to those in control patients. The left hemisphere had obvious activa-

tions in the inferior frontal, middle frontal, precentral, and supramarginal gyri, indicating that our patient had left-sided dominance of motor-language functions (Fig. 1B). In contrast, the abstract/concrete categorization task predominantly induced right-dominant activation in the temporal region, including the superior temporal and fusiform gyri (Fig. 1C). Based on these findings, we suggest that the language functions were separately distributed over both hemispheres.

TABLE 2

Results of the amobarbital test*

	Side of Test & Findings	
Item	Lt Injection	Rt Injection
paresis	rt hemi (4 mins)	lt hemi (4 mins, 30 secs)
counting	stopped (3 mins, 30 secs)	continued
letter-reading	71% (5 of 7)	14% (1 of 7)
naming	40% (2 of 5)	100% (5 of 5)
auditory comprehension	80% (4 of 5)	20% (1 of 5)
pointing to objects	100% (4 of 4)	25% (1 of 4)
general impression	impaired overt naming w/ severe dysarthria but little sensory aphasia	severe sensory aphasia w/ mild dysarthria

* Hemi = hemiparesis.

The expressive and receptive language functions were dissociated in the left frontal and right temporal lobes, respectively.

The MEG Profiles and Dipole Locations. The rate of successful task performance and the reaction time of the patient were within the control range. Figure 3A demonstrates the entire MEG view obtained in our patient, including the kana-reading task and the root mean squared fields in the bilateral frontotemporal and temporooccipital regions. Late deflections peaking at approximately 450 msec were more often observed in the right than in the contralateral frontotemporal region. There was no marked difference regarding side in the late responses in the temporooccipital regions. Estimated dipoles of the left frontotemporal responses were concentrated in the posterior part of the right superior temporal and middle temporal gyri (138 dipoles), which were adjacent to the posterior border of the tumor (Fig. 3B). In addition, another dipole cluster (64 dipoles) in the temporooccipital region was localized in the right fusiform gyrus. The total dipole number in the left hemisphere (48 dipoles) did not reach even a quarter of that in the right hemisphere, suggesting right-sided dominance of the reading process in this patient. The multiple current estimate analysis and the single equivalent dipole model demonstrated high current density spots in the posterior part of the right superior temporal and fusiform gyri. The figure-discrimination task evoked few late responses in either hemisphere. The second MEG performed on the 7th day before the operation yielded similar findings (right-sided dominance) in the temporoparietal regions.

A striking finding on the fMR imaging and MEG studies was that language functions in this patient might be dissociated over both hemispheres. We intended, therefore, to validate the neurological profiles with the amobarbital test before surgery.

The Amobarbital Test. The amobarbital test revealed left hemispheral dominance in all control patients, because the left ICA injection immediately disturbed all the motor and receptive-language functions.

Our patient stopped counting and failed to name objects (40%) after left ICA injection, whereas letter-reading (71%), auditory comprehension (80%), and pointing objects tasks (100%) were well preserved. In contrast, after right ICA injection, letter-reading (14%), auditory comprehen-

sion (20%), and pointing objects tasks (25%) were markedly suppressed, although the patient continued to count correctly without speech blockade (naming; 100%) but with slight hesitation. Detailed analysis of the results of the amobarbital test indicated interhemispheral dissociations of the expressive and receptive language functions (Table 2).

Operation. Although we obtained informed consent for radical resection of the tumor, the patient refused to undergo the awake surgical procedure. We therefore planned to perform tumor resection guided by the preoperative functional mapping. After integration of the lexicosemantic MEG dipoles into the neuronavigation system,[10] the insular cortex was exposed by a frontotemporal craniotomy. The tumor and involved brain tissue in the right anterior temporal and insular regions were removed in a gross-total fashion. We carefully spared suspected functional areas in the temporal lobe, where the MEG dipoles and the spots activated on fMR imaging were observed (Fig. 4). The histopathological diagnosis of this lesion was World Health Organization Grade II diffuse astrocytoma.

Postoperative Course. The patient awoke with slight, transient sensory aphasia after surgery. Although spontaneous speech and naming capacities were intact, mild sensory aphasia and dyslexia remained. Neuropsychological examinations conducted 4 months postsurgery disclosed slight impairment of vocabulary and comprehension, which resulted in deterioration of the patient's verbal IQ scores on the WAIS-R and the WAB tests (Table 1).

Discussion

The primary finding in this study was that the language dominance can be identified by combining different imaging methods. The use of fMR imaging with the verb-generation task detected the activation of the middle frontal and inferior frontal gyri, whereas MEG performed in conjunction with the kana-reading task localized the dipole clusters of the late responses in the superior temporal regions, such as the superior temporal and supramarginal gyri. These findings may mean that fMR imaging and MEG studies visualize independent centers for the expressive and receptive language functions in addition to indicating the language dominance. Particularly in our patient, fMR imaging and MEG studies demonstrated dissociated language functions over both hemispheres. The left frontal and right temporal regions took the expressive and receptive language roles, respectively. This unusual profile was consistently observed on repeated examinations and was finally validated by the results of the amobarbital test. After tumor resection, the patient experienced transient sensory aphasia for 1 week. Because the surgical procedure in the right frontotemporal region caused mild language deficits, the presence of aphasia supports the plausibility of the unusual functional profiles in this patient.

Kurthen, et al.,[13] first suggested the possibility of dissociated language functions when they used the amobarbital test to evaluate more than 100 patients with epilepsy. They reported on four patients with this disease who might have had independent frontal and temporal language centers in each hemisphere, and concluded that early-onset epilepsy might cause unusual representation of language functions. They did, however, find it difficult to distinguish the frontal

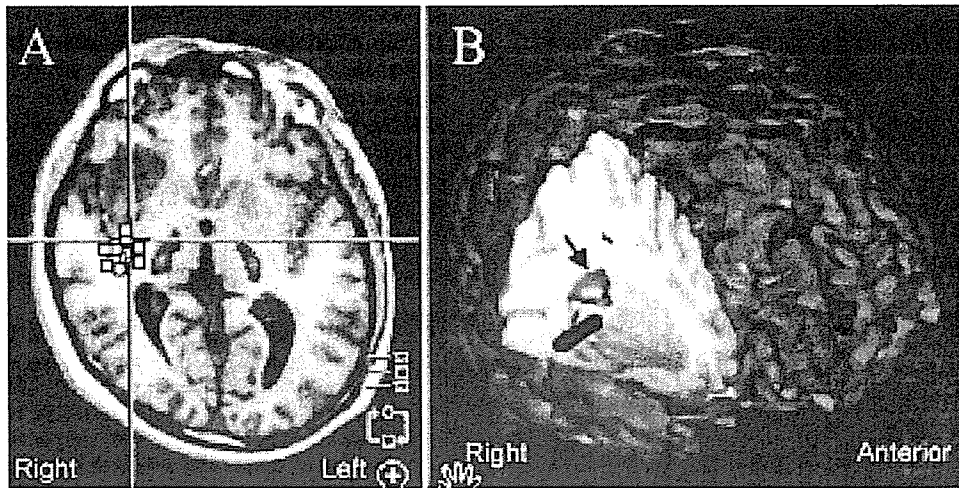Dissociated language functions on functional brain mapping

FIG. 4. A: Two-dimensional axial MR image demonstrating that the posterior border of resection is close to the dipole accumulation in the superior temporal region. B: Three-dimensionally reconstructed intracranial data obtained in our patient, clearly showing that a tip of the navigation probe (dark gray elongated oval) indicates the anterior border of lexicosemantic dipole clusters (arrow).

and temporal functions clearly because of the limited evaluation time associated with the amobarbital action and the level of patient cooperation. Noninvasive functional imaging techniques have recently become available to assess higher brain functions, and fMR imaging is becoming an alternative to the amobarbital test.[15,21,22] There have been few reports, however, of validations of the fMR imaging–activated areas by cortical stimulation.[22,24] It is still important to interpret fMR imaging results carefully by considering the results of the amobarbital test, electrocortical stimulation, and other functional imaging methods. Since the introduction of clinical fMR imaging, only four case reports have been published in which dissociated language functions were suggested (Table 3).[2,8,19,21]

Holodny, et al.,[8] and Baciu and colleagues[2] demonstrated translocation of the Broca area in isolation from temporal language function in patients with low-grade frontal glioma. Petrovich, et al.,[19] and Ries and coworkers[21] recently demonstrated that the temporal language function was translocated to the right hemisphere in patients with left temporal tumors. In their reports on fMR imaging, however, these investigators did not fully detail and confirm the unusual profiles with the amobarbital test. Using electrocortical stimulation, Baciu, et al., and Petrovich, et al., have observed no suppression of language function in frontal or temporal lobes containing tumors, findings that have caused them to stress the possibility of a functional dissociation.

Although fMR imaging–based brain mapping was used in all of these studies to investigate dissociation, in other reports researchers have found that even the various language tasks that are part of this modality produced little temporoparietal activation.[15,23,24] Rutten, et al.,[23,24] focused on the correspondence between fMR imaging and intraoperative electrocortical stimulation in the temporoparietal region. They applied several language tasks, such as picture naming, verbal fluency, and sentence comprehension, and concluded that much less activation appeared on fMR imaging in the temporoparietal than in the frontal area, but the physiological reason for this difference remains unknown. Be-

cause little neuronal activity is detected in the Wernicke areas on fMR imaging–based mapping, a more reliable method is required. One option that is highly complementary to fMR imaging is MEG. Simos and colleagues[25] have reported that the dipole localization of the lexicosemantic MEG in the temporoparietal region was reliable and showed excellent correlation with intraoperative cortical mapping. We believe that the combination of fMR imaging and MEG enables reliable identification of the expressive and receptive language functions.

In many previous reports, investigators have described either the shift or development of expressive and receptive language functions together in the expected nondominant right hemisphere.[1,5] Assuming that the dissociated language centers in our patient might reflect actual functional distributions, we must carefully consider the subcortical connections between the centers. Expressive and receptive language areas are usually connected by a large white-matter tract called the arcuate fasciculus. An arrangement in which the two language centers are in opposite hemispheres makes little physiological sense because it would involve a much more circuitous path of interaction between the centers. Recently developed diffusion tensor imaging might be used to clarify white-matter connections, such as the corpus callosum and the corticospinal tract. This technique, however, still has insufficient spatial resolution for small axonal bundles, including the anterior and posterior commissures. Although detailed physiological connections are still unclear, the technical development of diffusion tensor imaging might help resolve these issues in the near future.

Conclusions

Bilateral language dominance, which was generally determined with the amobarbital test, may involve dissociated frontal and temporal language functions. A slow-growing brain tumor or early-onset epilepsy might induce this unusual functional distribution. In our patient there remains speculation that the growth of the brain tumor prevented the

TABLE 3
Literature review of reports of dissociated language function*

Authors & Year	Patient Age (yrs), Sex; Hand	Patient Symptoms & Duration (yrs)	Patient Tumor Location	Dominance on fMRI Front-al	Dominance on fMRI Tem-poral	Amobarbital Test Expres-sive	Amobarbital Test Re-ceptive	Dominance on MEG (reading task)	Cortical Stimulation & Effect	Postop Course
Holodny, et al., 2002	34, M; rt	mild rt hemi, dysarthria (7)	lt insular (astrocytoma)	rt	lt	ND	ND	ND	ND	improved
Baciu et al., 2003	30, M; lt	epilepsy, apraxia (26)	lt frontal (ganglioglioma)	rt	lt	failed†	failed†	ND	lt frontal (none)	no change
Petrovich, et al., 2004	62, M; rt	none	lt temporoparietal (astrocytoma)	lt	rt	ND	ND	ND	lt frontal (arrest); lt temporal (none)	improved
Ries, et al., 2004	13, F; ambi	epilepsy (10)	lt temporal (subependymoma)	lt	rt	rt	rt	ND	ND	improved
present study	29, M; rt	transient amnesia (~11)	rt insular (astrocytoma)	lt	rt	lt	rt	rt	ND	mild sensory aphasia

* Ambi = ambidextrous; hand = handedness; ND = not done.
† The amobarbital test failed to show dominance.

involved area from functioning properly and led to transfer of the expressive language function to the contralateral (left) side. On the other hand, this unusual functional organization may have been congenital. The reason for the dissociation, however, cannot be definitively determined. Based on our findings in this case, we would like to stress that the combination of fMR imaging and MEG studies can be used to identify functional characteristics in individual patients.

References

1. Abo M, Senoo A, Watanabe S, Miyano S, Doseki K, Sasaki N, et al: Language-related brain function during word repetition in post-stroke aphasics. Neuroreport 15:1891–1894, 2004
2. Baciu MV, Watson JM, McDermott KB, Wetzel RD, Attarian H, Moran CJ, et al: Functional MRI reveals an interhemispheric dissociation of frontal and temporal language regions in a patient with focal epilepsy. Epilepsy Behav 4:776–780, 2003
3. Branch C, Milner B, Rasmussen T: Intracarotid sodium amytal for the lateralization of cerebral speech dominance; observations in 123 patients. J Neurosurg 21:399–405, 1964
4. Chen HM, Varshney PK: Mutual information-based CT-MR brain image registration using generalized partial volume joint histogram estimation. IEEE Trans Med Imaging 22:1111–1119, 2003
5. Fernandez B, Cardebat D, Demonet JF, Joseph PA, Mazaux JM, Barat M, et al: Functional MRI follow-up study of language processes in healthy subjects and during recovery in a case of aphasia. Stroke 35:2171–2176, 2004
6. Helmstaedter C, Kurthen M, Linke DB, Elger CE: Patterns of language dominance in focal left and right hemisphere epilepsies: relation to MRI findings, EEG, sex, and age at onset of epilepsy. Brain Cogn 33:135–150, 1997
7. Holodny AI, Schulder M, Liu WC, Maldjian JA, Kalnin AJ: Decreased BOLD functional MR activation of the motor and sensory cortices adjacent to a glioblastoma multiforme: implications for image-guided neurosurgery. AJNR 20:609–612, 1999
8. Holodny AI, Schulder M, Ybasco A, Liu WC: Translocation of Broca's area to the contralateral hemisphere as the result of the growth of a left inferior frontal glioma. J Comput Assist Tomogr 26:941–943, 2002
9. Kamada K, Houkin K, Iwasaki Y, Takeuchi F, Kuriki S, Mitsumori K, et al: Rapid identification of the primary motor area by using magnetic resonance axonography. J Neurosurg 97:558–567, 2002
10. Kamada K, Houkin K, Takeuchi F, Ishii N, Ikeda J, Sawamura Y, et al: Visualization of the eloquent motor system by integration of MEG, functional, and anisotropic diffusion-weighted MRI in functional neuronavigation. Surg Neurol 59:352–362, 2003
11. Kamada K, Kober H, Saguer M, Moller M, Kaltenhauser M, Vieth J: Responses to silent Kanji reading of the native Japanese and German in task subtraction magnetoencephalography. Brain Res Cogn Brain Res 7:89–98, 1998
12. Kamada K, Sawamura Y, Takeuchi F, Houkin K, Kawaguchi H, Iwasaki Y, et al: Gradual recovery from dyslexia and related serial magnetoencephalographic changes in the lexicosemantic centers after resection of a mesial temporal astrocytoma. Case report. J Neurosurg 100:1101–1106, 2004
13. Kurthen M, Helmstaedter C, Linke DB, Solymosi L, Elger CE, Schramm J: Interhemispheric dissociation of expressive and receptive language functions in patients with complex-partial seizures: an amobarbital study. Brain Lang 43:694–712, 1992
14. Lehericy S, Biondi A, Sourour N, Vlaicu M, du Montcel ST, Cohen L, et al: Arteriovenous brain malformations: is functional MR imaging reliable for studying language reorganization in patients? Initial observations. Radiology 223:672–682, 2002
15. Lehericy S, Cohen L, Bazin B, Samson S, Giacomini E, Rougetet

R, et al: Functional MR evaluation of temporal and frontal language dominance compared with the Wada test. Neurology 54: 1625–1633, 2000

16. Masutani Y, Aoki S, Abe O, Hayashi N, Otomo K: MR diffusion tensor imaging: recent advance and new techniques for diffusion tensor visualization. Eur J Radiol 46:53–66, 2003

17. Papanicolaou AC, Simos PG, Breier JI, Zouridakis G, Willmore LJ, Wheless JW, et al: Magnetoencephalographic mapping of the language-specific cortex. J Neurosurg 90:85–93, 1999

18. Papanicolaou AC, Simos PG, Castillo EM, Breier JI, Sarkari S, Pataraia E, et al: Magnetocephalography: a noninvasive alternative to the Wada procedure. J Neurosurg 100:867–876, 2004

19. Petrovich NM, Holodny AI, Brennan CW, Gutin PH: Isolated translocation of Wernicke's area to the right hemisphere in a 62-year-man with a temporo-parietal glioma. AJNR 25:130–133, 2004

20. Rasmussen T, Milner B: The role of early left-brain injury in determining lateralization of cerebral speech functions. Ann N Y Acad Sci 299:355–369, 1977

21. Ries ML, Boop FA, Griebel ML, Zou P, Phillips NS, Johnson SC, et al: Functional MRI and Wada determination of language lateralization: a case of crossed dominance. Epilepsia 45:85–89, 2004

22. Roux FE, Boulanouar K, Lotterie JA, Mejdoubi M, LeSage JP, Berry I: Language functional magnetic resonance imaging in preoperative assessment of language areas: correlation with direct cortical stimulation. Neurosurgery 52:1335–1347, 2003

23. Rutten GJ, Ramsey NF, van Rijen PC, Alpherts WC, van Veelen CW: FMRI-determined language lateralization in patients with unilateral or mixed language dominance according to the Wada test. Neuroimage 17:447–460, 2002

24. Rutten GJ, Ramsey NF, van Rijen PC, Noordmans HJ, van Veelen CW: Development of a functional magnetic resonance imaging protocol for intraoperative localization of critical temporoparietal language areas. Ann Neurol 51:350–360, 2002

25. Simos PG, Papanicolaou AC, Breier JI, Wheless JW, Constantinou JE, Gormley WB, et al: Localization of language-specific cortex by using magnetic source imaging and electrical stimulation mapping. J Neurosurg 91:787–796, 1999

26. Stenbacka L, Vanni S, Uutela K, Hari R: Comparison of minimum current estimate and dipole modeling in the analysis of simulated activity in the human visual cortices. Neuroimage 16:936–943, 2002

27. Yetkin FZ, Mueller WM, Morris GL, McAuliffe TL, Ulmer JL, Cox RW, et al: Functional MR activation correlated with intraoperative cortical mapping. AJNR 18:1311–1315, 1997

ORIGINAL PAPER

Kazuhiko Mishima · Yukinari Kato · Mika Kato Kaneko
Ryo Nishikawa · Takanori Hirose · Masao Matsutani

Increased expression of podoplanin in malignant astrocytic tumors as a novel molecular marker of malignant progression

Abstract Podoplanin (aggrus) is a mucin-like transmembrane sialoglycoprotein that is expressed on lymphatic endothelial cells. Podoplanin is putatively involved in cancer cell migration, invasion, metastasis, and malignant progression and may be involved in platelet aggregation. Previously, we showed upregulated expression of podoplanin in central nervous system (CNS) germinomas, but not in non-germinomatous germ cell tumors, except for parts of immature teratomas in limited numbers. However, little information exists about its role in CNS astrocytic tumors. In this study, 188 astrocytic tumors (30 diffuse astrocytomas, 43 anaplastic astrocytomas, and 115 glioblastomas) were investigated using immunohistochemistry with an anti-podoplanin antibody, YM-1. In 11 of 43 anaplastic astrocytomas (25.6%) and in 54 of 115 glioblastomas (47.0%), podoplanin was expressed on the surface of anaplastic astrocytoma cells and glioblastoma cells, especially around necrotic areas and proliferating endothelial cells. However, the surrounding brain parenchyma was not stained by YM-1. On the other hand, podoplanin expression was not observed in diffuse astrocytoma (0/30: 0%). Furthermore, we investigated the expression of podoplanin using quantitative real-time PCR and Western blot analysis in 54 frozen astrocytic tumors (6 diffuse astrocytomas, 14 anaplastic astrocytomas, and 34 glioblastomas). Podoplanin mRNA and protein expression were markedly higher in glioblastomas than in anaplastic astrocytomas. These data suggest that podoplanin expression might be associated with malignancy of astrocytic tumors.

Keywords Podoplanin · Astrocytoma · Glioblastoma · YM-1

K. Mishima · R. Nishikawa · M. Matsutani
Department of Neurosurgery, Saitama Medical School,
38 Morohongo Moroyama-machi Iruma-gun,
Saitama 350-0495, Japan

Y. Kato (✉) · M. K. Kaneko
Research Center for Glycoscience,
National Institute of Advanced Industrial Science and
Technology (AIST), Open Space Laboratory C-2,
1-1-1 Umezono, Tsukuba, Ibaraki 305-8568, Japan
E-mail: yukinari-k@bea.hi-ho.ne.jp
Tel.: +81-29-8613197
Fax: +81-29-8613191

T. Hirose
Department of Pathology, Saitama Medical School,
38 Morohongo Moroyama-machi Iruma-gun,
Saitama 350-0495, Japan

Introduction

Astrocytic tumors are the most common tumors of the central nervous system (CNS) and are categorized into diffuse astrocytomas (World Health Organization (WHO) Grade II), anaplastic astrocytomas (AA; WHO Grade III) and glioblastomas (GBM; WHO Grade IV) [11]. Among them, GBMs are the most frequent and most malignant type of astrocytic tumor. Despite advances in surgical techniques, radiation therapy, and adjuvant chemotherapy, their prognosis remains poor: the median survival time for patients with GBMs is only 1 year [2]. Glioblastoma may occur de novo or may result from progression of low-grade astrocytomas [4]. Molecular mechanisms of tumorigenesis and malignant progression are associated with the inactivation of tumor suppressor genes such as p53-Rb pathway or the overexpression of oncogenes such as epidermal growth factor receptor [10]. However, the mechanisms of tumorigenesis and progression of astrocytic tumors have not been resolved. Identification of genes that are expressed differentially in high-grade astrocytomas, low-grade tumors, or normal brain tissues is important to elucidate the molecular mechanisms of tumorigenesis and to develop novel therapeutic strategies.

Podoplanin was reported to be expressed in lymphatic endothelium and in tumor-associated lymphangiogenesis; also, podoplanin deficiency resulted in congenital lymphedema and impaired lymphatic vascular patterning [16]. Furthermore, expression of podoplanin has been

shown to be upregulated in skin squamous cell carcinoma [12], lung squamous cell carcinoma [9], malignant mesothelioma [14], Kaposi's sarcoma, angiosarcoma [1], hemangioblastoma [15], testicular seminoma [7, 8], and dysgerminoma [17].

We have recently shown that podoplanin is overexpressed in CNS germinomas, but not in non-germinomatous germ cell tumors, except in a limited number of immature teratomas with partial positive reactivity [13]. In adult non-neoplastic CNS, podoplanin was evident in the subependymal areas, the leptomeninges, choroid plexus, ependyma, and Purkinje cells [15, 17]. However, podoplanin expression in CNS astrocytic tumors has not been studied intensively. In this study, we investigated podoplanin expression in 188 astrocytic tumors.

Materials and methods

Tissue samples

Tumor specimens were obtained during surgery from eight patients with diffuse astrocytomas, 14 patients with anaplastic astrocytomas, and 34 patients with glioblastomas. Informed consent had been obtained previously from patients or their guardians. The tumor specimens were routinely fixed in 10% buffered formalin for 18–20 h at room temperature and processed to paraffin. Sections (5 μm thick) were cut and attached to poly-L-lysine-coated glass slides. Hematoxylin-eosin was used for routine staining. Tissue microarrays of 132 astrocytic tumors (22 diffuse astrocytomas, 29 anaplastic astrocytomas, and 81 glioblastomas) were purchased from Cybrdi, Inc. (Frederick, MD). The histology of these tissue samples was confirmed by experienced neuropathologists.

Immunohistochemical analysis

Specimens were deparaffinized, rehydrated, and incubated first with YM-1 (1/100 diluted; Medical Biological Laboratories Co., Ltd, Nagoya, Japan) at room temperature for 1 h, then with biotin-conjugated secondary anti-rat IgG antibody (DakoCytomation, Glostrup, Denmark) for 1 h, and finally with peroxidase-conjugated biotin–streptavidin complex (Vectastain ABC Kit; Vector Laboratories, Inc., Burlingame, CA) for 1 h. Color was developed using 3,3-diaminobenzidine tetrahydrochloride tablet sets (DakoCytomation) for 3 min. Podoplanin expression was assessed semi-quantitatively from the percentage of tumor cells with cytoplasmic/membrane staining: 0, no staining; +, <10%; ++, 10–50%; and +++, >50%.

Western blot analysis

Tissues were solubilized with lysis buffer (25 mM Tris (pH 7.4), 50 mM NaCl, 0.5% Na deoxycholate, 2% nonidet P-40, 0.2% SDS, 1 mM phenylmethylsulfonyl fluoride, and 50 mg/ml aprotinin). They were then electrophoresed under reducing conditions on 10–20% polyacrylamide gels (Daiichi Pure Chemicals Co., Ltd, Tokyo, Japan). The separated proteins were transferred to a nitrocellulose membrane. After blocking with 4% skim milk in PBS, the membrane was incubated with YM-1 (1/500 diluted) or anti-β-actin antibody (1 μg/ml; Sigma Chemical Co., St. Louis, MO), and then with peroxidase-conjugated secondary antibodies (1/1,000 diluted; Amersham Pharmacia Biotech UK Ltd, Buckinghamshire, UK). The proteins were subsequently developed for 3 min using ECL reagents (Amersham Pharmacia Biotech) using X-Omat AR film (Eastman Kodak Co.).

Quantitative real-time PCR

Total RNAs were prepared from frozen sections that have been obtained from astrocytic tumor patients, employing an RNeasy mini prep kit (Qiagen, Inc., Hilden, Germany). The initial cDNA strand was synthesized using SuperScript III transcriptase (Invitrogen Co., Carlsbad, CA) by priming nine random oligomers and an oligo-dT primer according to the manufacturer's instructions. We performed PCR using oligonucleotides: human podoplanin sense (5′-GGAAGGTGTCAGCT CTGCTC-3′) and human podoplanin antisense (5′-CG CCTTCCAAACCTGTAGTC-3′). Real-time PCR was carried out using the QuantiTect SYBR Green PCR (Qiagen, Inc.). The PCR conditions were 95°C for 15 min (1 cycle), followed by 40 cycles of 94°C for 15 s, 53°C for 20 s, 72°C for 10 s. Subsequently, a melting curve program was applied with continuous fluorescence measurement. A standard curve for podoplanin templates was generated through serial dilution of PCR products (1×10^8–1×10^2 copies/μl). The expression level of podoplanin was normalized by total RNA weights. The statistical signifi cance of podoplanin mRNA expression in astrocytic tumor tissues was determined using paired t tests.

Results

Immunohistochemical staining for podoplanin in malignant astrocytic tumors

The cellular distribution of podoplanin in astrocytic tumors was examined immunohistochemically using anti-podoplanin antibody, YM-1, which can strongly recognize podoplanin [6, 13]. In this study, we used 56 surgical tissues (8 diffuse astrocytomas, 14 anaplastic astrocytomas, and 34 glioblastomas). Podoplanin immunoreactivity was detected in 5 of 14 (35.7%) anaplastic astrocytomas and in 18 of 34 (52.9%) glioblastomas; staining was graded as +++ in 16 glioblastomas and as ++ in two glioblastoma cases. We also stained other astrocytic tumors of tissue microarrays. Podoplanin was detected in 6 of 29 (21%) anaplastic astrocytomas and in 36 of 81 (44%) glioblastomas. In all, 11 of 43 anaplastic

astrocytomas (25.6%) and 54 of 115 (47.0%) glioblastomas were stained using YM-1 (χ^2, $P<0.05$; Table 1). Representative staining for podoplanin in glioblastoma samples is shown in Fig. 1. Immunostaining for podoplanin demonstrated predominantly cell surface patterns in glioblastoma cells (Fig. 1). In anaplastic astrocytoma, the tumor cell surface was stained using YM-1 (Fig. 1c, d). In glioblastomas, podoplanin-positive tumor cells were prominent around microvascular proliferations (Fig. 1e, f) and necrotic tissues (Fig. 1g). Proliferating endothelial cells were negative for podoplanin (Fig. 1e, f). Podoplanin was detected strongly in the plasma membrane of highly anaplastic multinucleated giant cells (Fig. 1h). In non-neoplastic areas of the brain (Fig. 1a) and in diffuse astrocytoma (Fig. 1b), podoplanin immunostaining was absent.

Podoplanin expression in malignant astrocytic tumors using Western blot analysis

To confirm immunohistochemical findings from astrocytic tumors, lysates of frozen tumor specimens from 54 patients (6 diffuse astrocytomas, 14 anaplastic astrocytomas, and 34 glioblastomas) were analyzed using Western blotting. As shown in Fig. 2, an antibody to podoplanin, YM-1, detected about 36-kDa proteins in extracts of malignant astrocytomas. Using YM-1, 6 of 14 anaplastic astrocytomas (42.8%) and 22 of 34 glioblastomas (64.7%) showed strong labeling (χ^2, $P<0.05$), while all diffuse astrocytomas were negative. Podoplanin expression detected by Western blot analysis was closely correlated with the results of immunohistochemistry.

Differential expression of podoplanin mRNA in astrocytic tumors

To quantify the expression of podoplanin mRNA in human astrocytic tumors of different grades, we performed quantitative real-time PCR analyses of astrocytic tumors from 54 patients (6 diffuse astrocytomas, 14 anaplastic astrocytomas, and 34 glioblastomas). The relative podoplanin mRNA expression levels of each tumor grade are shown in Fig. 3. Average copies of podoplanin mRNA/μg total RNA in diffuse astrocytomas (Grade II), anaplastic astrocytomas (Grade III), and glioblastomas (Grade IV) were 21.7±30.6, 16.1±35.4, and 411.2± 511.7, respectively. Podoplanin transcript levels were significantly higher in glioblastomas than those in diffuse astrocytomas, anaplastic astrocytomas, or non-neoplastic human brain tissues ($P<0.01$).

Discussion

Immunohistochemical, Western blot, and real-time PCR analyses demonstrate that the expressions of podoplanin mRNA and protein are correlated with the malignant progression from anaplastic astrocytoma (Grade III) to glioblastomas (Grade IV). Of particular interest, 47.0% of highly invasive glioblastomas express podoplanin, whereas 25.6% of anaplastic astrocytomas and 0% of the less invasive diffuse astrocytomas (Grade II) express podoplanin by immunohistochemical staining on surgically resected and microarray tissues (Table 1). On the other hand, 6 of 14 anaplastic astrocytomas (42.8%) and 22 of 34 glioblastomas (64.7%) were strongly labeled by Western blot analyses using YM-1 (Fig. 2). Of all 188 astrocytic tumors analyzed immunohistochemically, 132 cases were derived from tissue microarrays whose tissue spots are small and, therefore, the percentage of podoplanin-positive tumors might have been underestimated. Furthermore, YM-1 detected podoplanin strongly by Western blot analysis, as described previously [6]. For these reasons, podoplanin-positive ratios in immunohistochemical analysis are inferred to be smaller than those of Western blot analysis, although the expression of podoplanin detected by immunohistochemistry was closely correlated with that by Western blot or real-time PCR analyses. The distribution of podoplanin-positive tumor cells was prominent around necrotic tissue and proliferating endothelial cells in glioblastomas (Fig. 1). Normal brain tissue surrounding the tumor bed was negative for podoplanin. Therefore, podoplanin expression was correlated with high tumor grades and aggressive histological behavior.

The biological functions of podoplanin remain largely unknown. In vascular endothelial cells, overexpression of T1α/podoplanin induces elongated cell extensions and considerably increases cell adhesion, migration, and tube

Tumor type	No. of cases	Podoplanin immunostaining				Positive rate (%)
		+++	++	+	−	
Diffuse astrocytoma	30	0	0	0	30	0
Surgical resection samples	8	0	0	0	8	0
Tissue microarray	22	0	0	0	22	0
Anaplastic astrocytoma	43	6	3	2	32	25.6
Surgical resection samples	14	3	1	1	9	35.7
Tissue microarray	29	3	2	1	23	20.7
Glioblastoma	115	39	10	5	61	47
Surgical resection samples	34	16	2	0	16	52.9
Tissue microarray	81	23	8	5	45	44

Table 1 Results of podoplanin immunostaining in 188 patients with astrocytic tumors
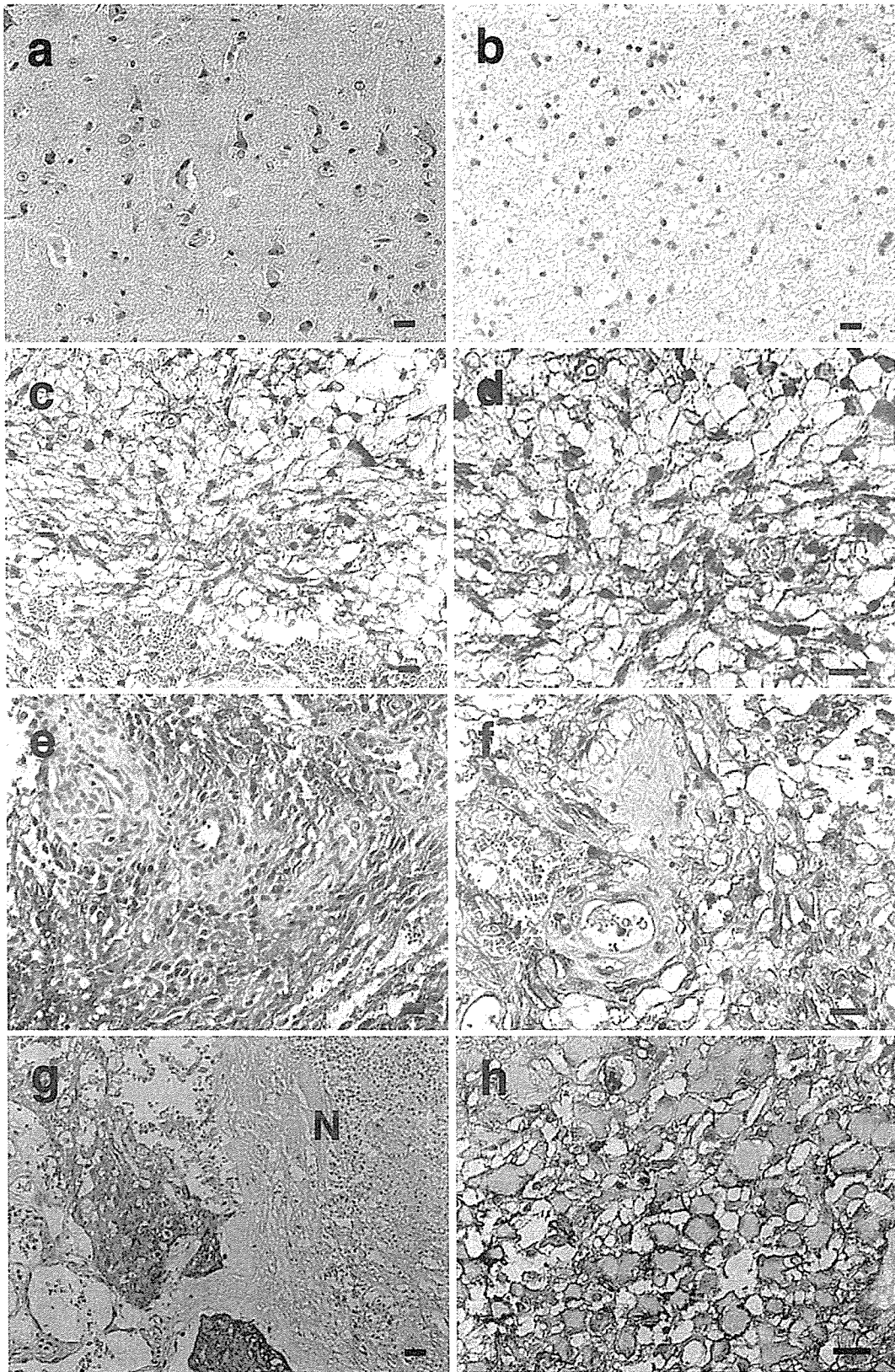
Fig. 1 Immunohistochemical detection of podoplanin in astrocytic tumors. No staining is apparent in a normal brain (**a**, ×200) and in diffuse astrocytoma (**b**, ×200). In anaplastic astrocytoma, the tumor cell surface was stained positively (**c**, ×200; **d**, ×400). Accentuated staining is visible around an area of microvascular proliferation in glioblastoma (**e**, ×200; **f**, ×400). Podoplanin immunostaining of glioblastoma cells at the necrotic area (*N*) (**g**, ×200) and in the plasma membrane of highly anaplastic multinucleated giant cells (**h**, ×400). *Bar* = 10 μm